

# DNA methylation regulator-mediated modification patterns and tumor microenvironment characterization in gastric cancer

Qi Meng,<sup>1,2,6</sup> Yun-Xin Lu,<sup>1,2,3,6</sup> Dan-Yun Ruan,<sup>1,4,6</sup> Kai Yu,<sup>1,2</sup> Yan-Xing Chen,<sup>1,2</sup> Min Xiao,<sup>5</sup> Yun Wang,<sup>1,2,3</sup> Ze-Xian Liu,<sup>1,2</sup> Rui-Hua Xu,<sup>1,2,3</sup> Huai-Qiang Ju,<sup>1,2</sup> and Miao-Zhen Qiu<sup>1,2,3</sup>

<sup>1</sup>State Key Laboratory of Oncology in South China, Collaborative Innovation Center for Cancer Medicine, Sun Yat-sen University Cancer Center, Guangzhou 510060, P.R. China; <sup>2</sup>Research Unit of Precision Diagnosis and Treatment for Gastrointestinal Cancer, Chinese Academy of Medical Sciences, Guangzhou 510060, P.R. China; <sup>3</sup>Department of medical oncology, Sun Yat-sen University Cancer Center, Guangzhou 510060, P.R. China; <sup>4</sup>Department of Medical Oncology, The Third Affiliated Hospital of Sun Yat-sen University, Guangzhou, P.R. China; <sup>5</sup>Department of Rheumatology and Immunology, Third Affiliated Hospital of Sun Yat-sen University, 600 Tianhe Road, Guangzhou 510630, Guangdong, P.R. China

**Growing evidence implies a link between DNA methylation and tumor immunity/immunotherapy. However, the global influence of DNA methylation on the characteristics of the tumor microenvironment and the efficacy of immunotherapy remains to be clarified. In this study, we systematically evaluated the DNA methylation regulator patterns and tumor microenvironment characteristics of 1,619 gastric cancer patients by clustering the gene expression of 20 DNA methylation regulators. Three gastric cancer subtypes that had different DNA methylation modification patterns and distinct tumor microenvironment characteristics were recognized. Then, a DNA methylation score (DMS) was constructed to evaluate DNA methylation modification individually. High DMS was characterized by immune activation status, increased tumor mutation burden, and tumor neoantigens, with a favorable prognosis. Conversely, activation of the stroma and absence of immune cell infiltration were observed in the low DMS group, with relatively poor survival. High DMS was also certified to be correlated with enhanced efficacy of immunotherapy in four immune checkpoint blocking treatment cohorts. In conclusion, the characterization of DNA methylation modification patterns may help to enhance our recognition of the tumor immune microenvironment of gastric cancer and guide more personalized immunotherapy strategies in the future.**

## INTRODUCTION

As one of the best characterized epigenetic modifications, DNA methylation has been reported to be related to numerous biological processes.<sup>1,2</sup> 5mC, which means that DNA methylation occurs at the fifth carbon atom of the cytosine residues within CpG dinucleotides, represents the major form of DNA methylation modification in mammals.<sup>3</sup>

Gastric cancer (GC) is the fourth most common cancer and the second leading cause of tumor-related deaths worldwide.<sup>4</sup> Although great efforts have been devoted to the treatment of GC, effectively individual-

ized therapeutic strategies remain to be explored.<sup>5,6</sup> Several genes that play essential roles in the initiation and progression of GC were reported to be regulated by hypermethylation or hypomethylation of the promoter. For instance, Higashimori et al.<sup>7</sup> reported that FOXF2 was preferentially methylated in GC, which could suppress GC through the FOXF2/IRF2BPL/ $\beta$ -catenin signaling axis. In addition, approximately 9% of GC is found to have Epstein-Barr virus (EBV) infection.<sup>8</sup> The major epigenetic change in EBV-positive GC is aberrant CpG island hypermethylation in the promoter regions of several tumor suppressor genes, which are involved in cell cycle regulation, apoptosis, cell adhesion, metastases, and DNA repair pathways.<sup>9</sup>

Immune checkpoint blocking therapy has been demonstrated to improve survival across multiple tumor types, including GC.<sup>10–17</sup> However, the overall efficiency was less than 20%. The tumor mutation burden (TMB), PD-L1 expression, microsatellite instability (MSI) status, and EBV infection were reported as potential biomarkers that favor PD-1 blockade-based immunotherapy.<sup>18</sup> Growing evidence implies a link between DNA methylation and tumor immunity/immunotherapy.<sup>19–21</sup> For example, Xu and colleagues<sup>22</sup> found that the interferon (IFN)- $\gamma$ /JAK/STAT/TET2 signaling pathway is involved in tumor immunity, and stimulating TET2 activity could enhance anti-PD-L1 efficacy in solid tumors.<sup>23</sup> We have recently reported TET1 mutation as a potential biomarker for immune checkpoint blocking therapy across multiple cancers. However, to date,

Received 9 October 2020; accepted 31 March 2021;  
<https://doi.org/10.1016/j.omtn.2021.03.023>.

<sup>6</sup>These authors contributed equally

**Correspondence:** Miao-Zhen Qiu, State Key Laboratory of Oncology in South China, Collaborative Innovation Center for Cancer Medicine, Sun Yat-sen University Cancer Center, Guangzhou 510060, P.R. China.

**E-mail:** [qiumzh@sysucc.org.cn](mailto:qiumzh@sysucc.org.cn)

**Correspondence:** Huai-Qiang Ju, State Key Laboratory of Oncology in South China, Collaborative Innovation Center for Cancer Medicine, Sun Yat-sen University Cancer Center, Guangzhou 510060, P.R. China.

**E-mail:** [juhq@sysucc.org.cn](mailto:juhq@sysucc.org.cn)



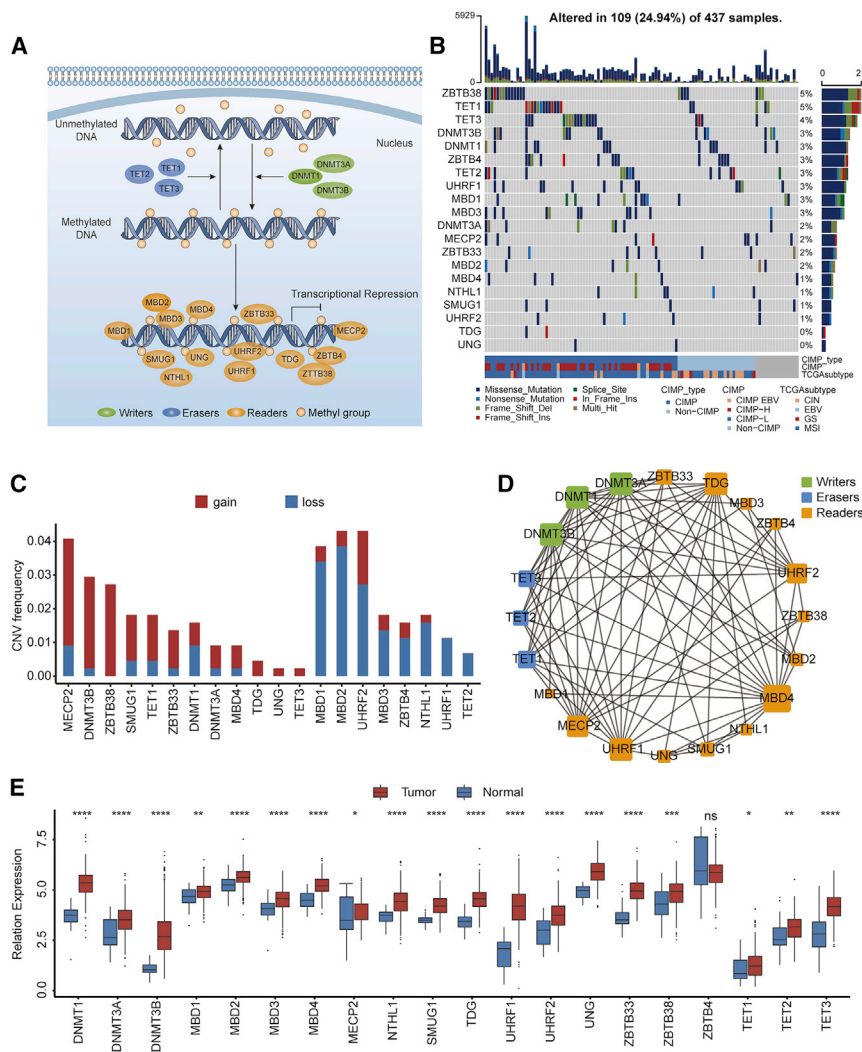


**Figure 1. Multi-omics landscape of DNA methylation regulators in GC**

(A) Overview of the 20 DNA methylation regulators and their major biological functions. (B) The mutation frequency of 20 DNA methylation regulators in TCGA STAD cohort. Each column of the figure represents an individual patient. The upper bar plot represents TMB. The number on the right shows the mutation frequency of each regulator. The right bar plot indicates the proportion of each variant type. The lower bar represents the sample annotations. (C) The CNV frequency of DNA methylation regulators in TCGA STAD cohort. Gain, red; loss, blue. (D) The protein-protein interaction network among DNA methylation regulators. The size of the node represents the number of proteins interacting with this modifier. (E) Boxplot shows the expression of 20 DNA methylation regulators between tumor and normal tissues in TCGA STAD cohort. \* $p < 0.05$ , \*\* $p < 0.01$ , \*\*\* $p < 0.001$ , \*\*\*\* $p < 0.0001$ .

## RESULTS

### Multi-omics landscape of DNA methylation regulators in GC

After systematic review of published articles about DNA methylation, a total of 20 DNA methylation regulators were collected and enrolled in our analysis, including 3 writers (DNMT1, DNMT3A, DNMT3B), 3 erasers (TET1, TET2, TET3), and 14 readers (MBD1, MBD2, MBD3, MBD4, ZBTB33, ZBTB38, ZBTB4, UHRF1, UHRF2, MECP2, UNG, TDG, NTHL1, SMUG1), as shown in Figure 1A.

The overall mutation rate of all regulators is relatively low in the GC genome (Figure 1B). Among all 20 modifiers, the eraser TET1, whose

mutation has been reported to be a favorable prognostic marker in patients receiving immunotherapy,<sup>22</sup> and the reader ZBTB38 had the highest mutation rates (5%), while two readers, TDG and UNG, exhibited extremely low mutation rates in GC patients (0%) (Figure 1B). Co-occurrence mutation patterns were found in several regulators, such as TET1 and DNMT1 or TET3 and DNMT3B, even though they might have opposite biological functions. However, no obvious mutation-exclusive phenomenon was found among these regulators (Figure S1B). For copy number variation (CNV), MECP2, DNMT3B, and ZBTB38 showed a relatively high frequency of amplification, while MBD1 and MBD2 were mainly copy number deletions (Figure 1C). The protein-protein interaction (PPI) network analyzed by STRING depicted widespread protein interactions among these modifiers (Figure 1D). As shown in Figure 1E, most regulators except ZBTB4 showed relatively higher RNA expression in tumors than in normal gastric tissues, indicating that they might play crucial roles in the initiation and progression of GC. Furthermore, most regulators presented obvious differential expression among distinct The Cancer

the global influence of all DNA methylation regulators on the immune microenvironment and the efficacy of immunotherapy remains unknown.

In this study, we integrated 1,619 patients from eight independent GC cohorts to identify DNA methylation regulator modification patterns by unsupervised clustering of the gene expression of 20 DNA methylation regulators. We chose to investigate the expression of genes that regulate DNA methylation rather than DNA methylation itself, since the function of DNA methylation can vary based on genomic context. Three distinct DNA methylation regulator patterns with different immune microenvironment characteristics were recognized and found to be consistent with the three classical immune phenotypes: immune-inflamed, immune-excluded, and immune desert. Importantly, a DNA methylation score (DMS) system was constructed to evaluate the DNA methylation status individually. Our results indicated that DMS may serve as an alternative biomarker for survival and efficacy of immunotherapy.

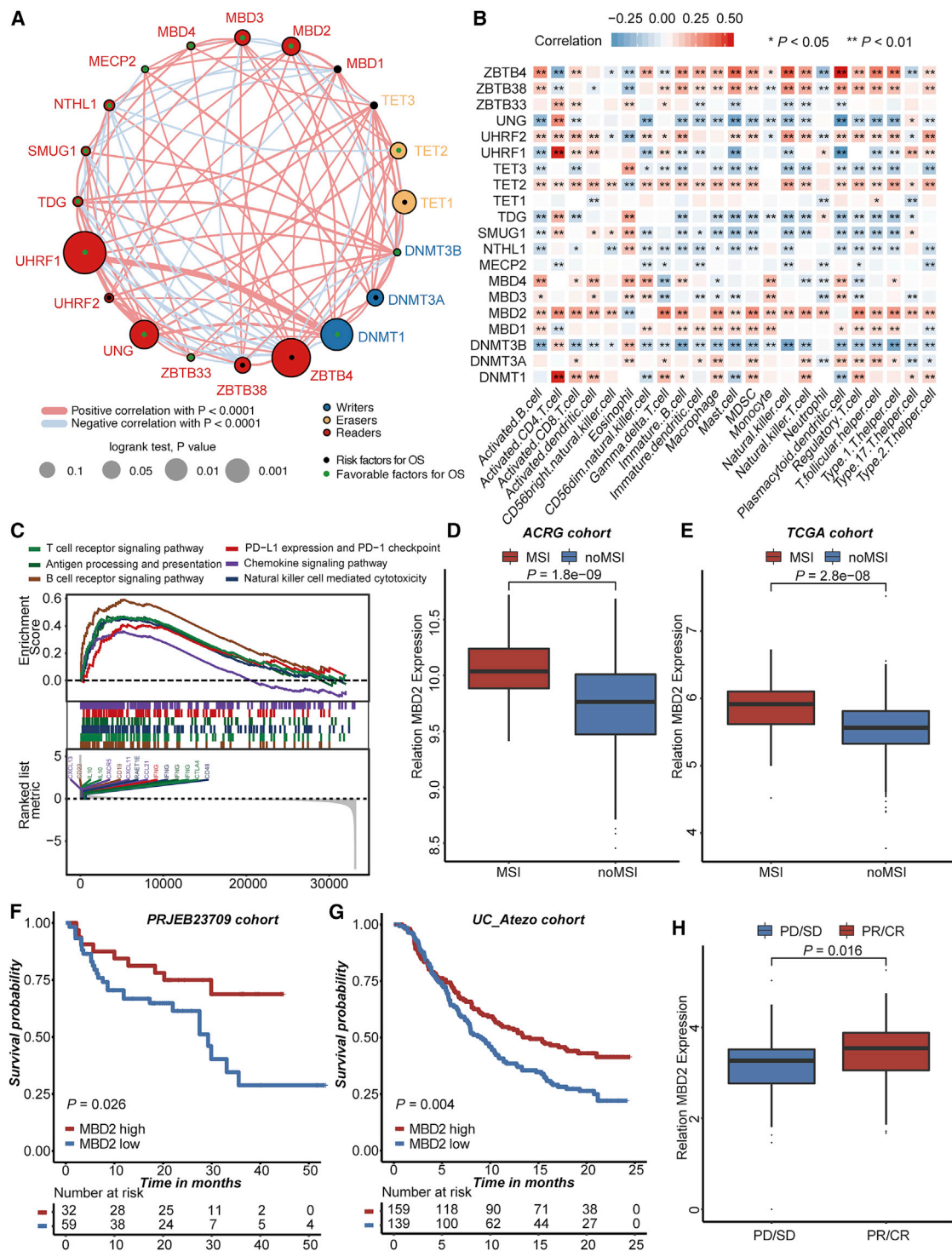


**Figure 2. Prognosis and immune characteristics of DNA methylation regulators**

(A) Correlations and prognosis of DNA methylation regulators in GC patients. The red line represents a positive correlation with  $p < 0.0001$ , and the blue line represents a negative correlation with  $p < 0.0001$ . The size of the node represents the p value of the log-rank test. Green points represent favorable factors for OS. Black points represent risk factors for OS. (B) Correlation heatmap between 20 DNA methylation regulators and immune cells in the gathered GC cohort. Orange indicates positive correlation; blue indicates negative correlation.  $*p < 0.05$ ,  $**p < 0.01$ . (C) GSEA analysis indicated that six immune/inflammation-related pathways were enriched in the MBD2-high expression

(legend continued on next page)

Genome Atlas (TCGA) molecular subtypes or CpG island methylator phenotype (CIMP) subtypes (Figures S1C and S1D). Also, some regulators individually or in combination were significantly associated with specific molecular subtypes or CIMP subtypes (Figures S1C and S1D), which indicated that they also contribute to the heterogeneity of GC. The results were also validated in the Asian Cancer Research Group (ACRG) cohort (Figure S1E). In addition, we speculated about the potential regulation of these regulators by promoter DNA methylation. We found a relatively strong negative correlation between the mean methylation of promoter sites and RNA expression for TET1 and TDG (Figures S1F and S1G). In conclusion, the above results revealed that crosstalk among these DNA methylation regulators might play crucial roles in the initiation, progression, and the heterogeneity of GC.

### Prognosis and immune characteristics of DNA methylation regulators

To further clarify the role of DNA methylation regulators in GC, we collected 1,619 patients with survival information from eight independent cohorts (Table S1), which is the largest GC cohort to our knowledge.

The probable molecular functions of these DNA methylation regulators were first investigated using 10 classical oncogenic pathways. Almost all regulators had a positive correlation with the cell cycle pathway (Figure S1H), which has been reported to be frequently dysregulated in cancer.<sup>24</sup> MBD1, ZBTB38, and ZBTB4 had a strong correlation with the transforming growth factor (TGF)- $\beta$  pathway, indicating the potential functions of these readers (Figure S1H). Further analysis of RNA expression revealed a relatively strong positive correlation among DNMT1, UHRF1, and UNG (Figure 2A; Table S2). The co-expression phenomenon of these genes might indicate a functional correlation, which needs further validation. The forest plot of a univariate Cox regression depicted the prognostic value of 20 DNA methylation modifiers (Figure S1I). The interactions and prognostic significance of these modifiers were further visualized in the network plot (Figure 2A).

DNA methylation has been reported to play significant roles in the immune system and tumor microenvironment.<sup>22,23</sup> Therefore, we also investigated the relationship between DNA methylation regulators and tumor immunology. The expression of MBD2, TET2, and DNMT1 was positively correlated with most immune cells (Figure 2B), which might explain their favorable prognostic value. It was also reported that patients with MSI status or EBV-positive phenotype usually had better immune checkpoint blockade treatment efficacy.<sup>25</sup> The expression of DNMT1, MBD2, UHRF1, UNG, and TET2 was significantly upregulated in the MSI group in both the

ACRG and TCGA cohorts (Figures S2A and S2B). The expression of DNMT1, DNMT3A, MBD2, MBD3, MBD4, NTHL1, and ZBTB4 was clearly high in the EBV-positive group (Figure S2C).

Considering the relatively higher correlation between MBD2 and activated CD8 T cells, and its favorable prognostic value, we further thoroughly analyzed the role of MBD2 in tumor immunology/immunotherapy. First, the MBD2 high-expression group had relatively higher immune cell infiltration abundance, especially for activated CD8<sup>+</sup> T cells, activated B cells, and activated CD4<sup>+</sup> T cells (Figure S2D). Second, gene set enrichment analysis (GSEA) analysis indicated that several immune or inflammation-related pathways, such as the T cell receptor signaling pathway, B cell receptor signaling pathway, antigen processing and presentation pathway, PD-L1 expression and PD-1 checkpoint pathway, chemokine signaling pathway, and natural killer (NK) cell-mediated cytotoxicity pathway, were significantly enriched in the MBD2 high-expression group (Figure 2C). Third, MBD2 had a relatively higher expression level not only in the MSI group, for both the ACRG (Figure 2D) and TCGA STAD (Figure 2E) cohorts, but also in the EBV-positive group (Figure S2C). Owing to the important role of MBD2 in tumor immunology, we also investigated whether the expression of MBD2 could help predict the efficacy of immune checkpoint blockade treatment. Survival analysis indicated that MBD2 high expression patients had better prognosis in the PRJEB23709 cohort (Figure 2F) and UC\_Atezo cohort (Figure 2G). Furthermore, the high expression of MBD2 represented a better clinical response (Figure 2H).

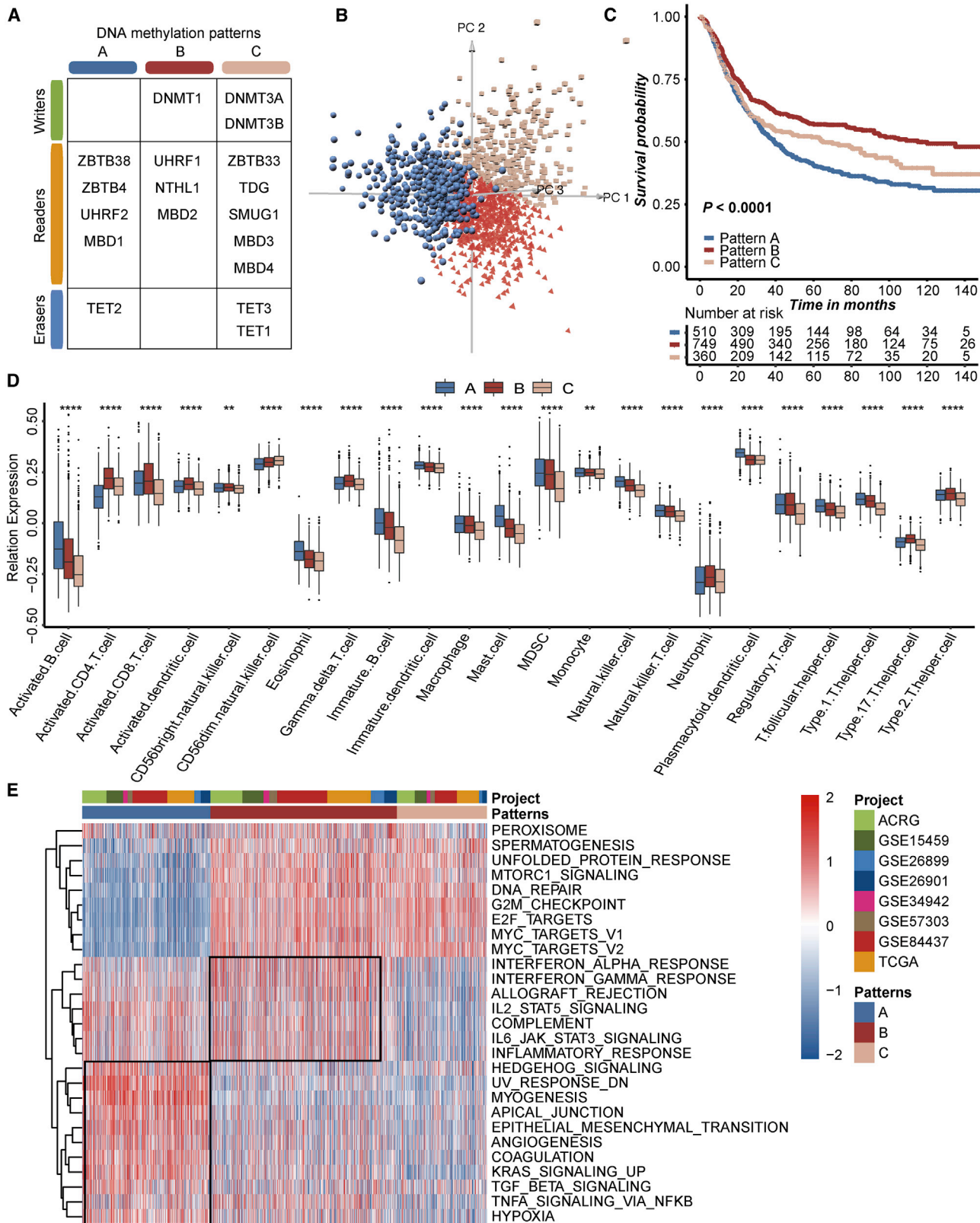
Above all, these results revealed the intimate relationship between DNA methylation regulators and the tumor microenvironment. The reader MBD2 was positively correlated with the infiltration of immune cells and might be a favorable biomarker for prognosis and the efficacy of immunotherapy in GC.

### DNA methylation modification patterns in the gathered GC cohort

As DNA methylation regulators might contribute to the heterogeneity of GC and they also were associated closely with the tumor microenvironment, to further recognize new probable DNA methylation regulator patterns, unsupervised clustering was conducted based on the expression of 20 DNA methylation regulators in the gathered GC cohort. As shown in Figure S3A, three clusters could achieve the best clustering efficacy. Accordingly, patients were classified into DNA methylation modification pattern A (n = 510), pattern B (n = 749), and pattern C (n = 360). DNA methylation regulator pattern A was characterized by high expression of ZBTB4, ZBTB38, MBD1, UHRF2, and TET2; DNA methylation regulator pattern B showed relatively high expression of UHRF1, DNMT1, UNG, and

---

group in the gathered GC cohort. The top of the figure represents the enrichment score of the pathways. The bottom of the figure represents the ranked differential expression gene list between the high and low MBD expression groups. (D) Boxplot of MBD2 expression between the MSI and no-MSI groups in the ACRG cohort. (E) Boxplot of MBD2 expression between the MSI and no-MSI groups in TCGA STAD cohort. (F) Overall survival analysis of high (n = 32) and low (n = 59) MBD2 expression groups in the PRJEB23709 immunotherapy cohort. Log-rank test, p = 0.026. (G) Boxplot of relative MBD2 expression for distinct clinical response groups. Kruskal-Wallis test, p = 0.016. (H) Overall survival analysis of high (n = 159) and low (n = 139) MBD2 expression groups in the UC\_Atezo immunotherapy cohort. Log-rank test, p = 0.0042.



(legend on next page)

NTHL1; DNA methylation regulator pattern C showed relatively high expression of ZBTB33, TET3, TET1, TDG, DNMT3A, DNMT3B, and MBD3 (Figures 3A, S3B, and S3C). Three-dimensional principal component analysis (3D-PCA) for the expression of 20 DNA methylation modifiers to distinguish three DNA methylation regulator patterns showed that three groups were obviously separated, indicating that they were well distinguished based on the expression of 20 DNA methylation regulators (Figure 3B). Survival analysis indicated that DNA methylation regulator pattern B was correlated with a notably favorable prognosis (Figure 3C) in accordance with its highest activated CD8 T cell, activated CD4 T cell, and activated dendritic cell infiltration (Figure 3D; Table S3).

Then, we explored the differences in signaling pathways among the three DNA methylation regulator patterns. DNA methylation regulator pattern B was enriched in immune/inflammation-related pathways, such as the IFN- $\gamma$  pathway, interleukin (IL)-6/JAK/STAT3 pathway, inflammatory response pathway, and complement pathway (Figure 3E; Table S4), indicating an immune/inflammation activation status in pattern B. DNA methylation regulator pattern A represented a stroma activation phenotype, with many enriched pathways, such as the epithelial-mesenchymal transition (EMT) pathway, hypoxia pathway, TGF- $\beta$  pathway, and angiogenesis pathway (Figure 3E).

#### Different clinical and transcriptome characteristics of the three DNA methylation regulator patterns in the ACRG cohort

To further explore the potential DNA methylation regulator patterns in GC, we focused our attention on the ACRG cohort, which had the most comprehensive clinical information. Unsupervised clustering of the gene expression of 20 DNA methylation regulators in the ACRG cohort also identified three DNA methylation-related patterns (Figures 4A, S4A, and S4D). The composition of DNA methylation regulators in the three patterns was almost similar to that of the gathered cohort (Figure S4E).

PCA in the ACRG cohort also indicated that patients were well distinguished based on the expression of 20 DNA methylation regulators (Figure S4F). Survival analysis revealed that DNA methylation regulator pattern B showed a significantly more favorable prognosis than did patterns A and C (Figure 4B, B versus A,  $p = 0.00016$ , B versus C,  $p = 0.00232$ ), in accordance with its highest activated CD8 T cell, activated CD4 T cell, and activated dendritic cell infiltration (Figure S4G). However, DNA methylation regulator pattern A did not exhibit a survival advantage over pattern C (Figure 4B,  $p = 0.70553$ ), even though pattern A also had obvious CD8 T cell and B cell infiltration (Figure S4G). Previous studies reported that TGF- $\beta$  could restrain the

antitumor immune response by restricting T cell infiltration.<sup>26</sup> We speculated that the stroma surrounding the tumor, which inhibited the infiltration of immune cells, caused poor prognosis of DNA methylation pattern A. Therefore, we identified several immune infiltration-related signatures from Mariathasan et al.'s<sup>26</sup> study (Table S5) and analyzed their association with DNA methylation regulator patterns. The results confirmed that pattern B was enriched in immune activation signatures such as CD8 T effector, co-stimulation antigen-presenting cell (APC), immune checkpoint, and type I IFN responses. Pattern A represented a stroma activation phenotype, with many signatures, such as angiogenesis, pan-F-TBRS, and EMT1-3 (Figure 4C). In line with the characteristics of immune cell infiltration and immune signatures, many stimulatory immunomodulators or immune checkpoint molecules were generally unregulated in DNA methylation regulator pattern B, indicating a relatively hot tumor immune microenvironment (Figure 4D). Moreover, based on the molecular subtypes of the ACRG cohort, we found that most patients of the MSI subtype were classified into pattern B, while most patients of the EMT subtype belonged to pattern A, which further confirmed the conclusion (Figures 4E and S4H).

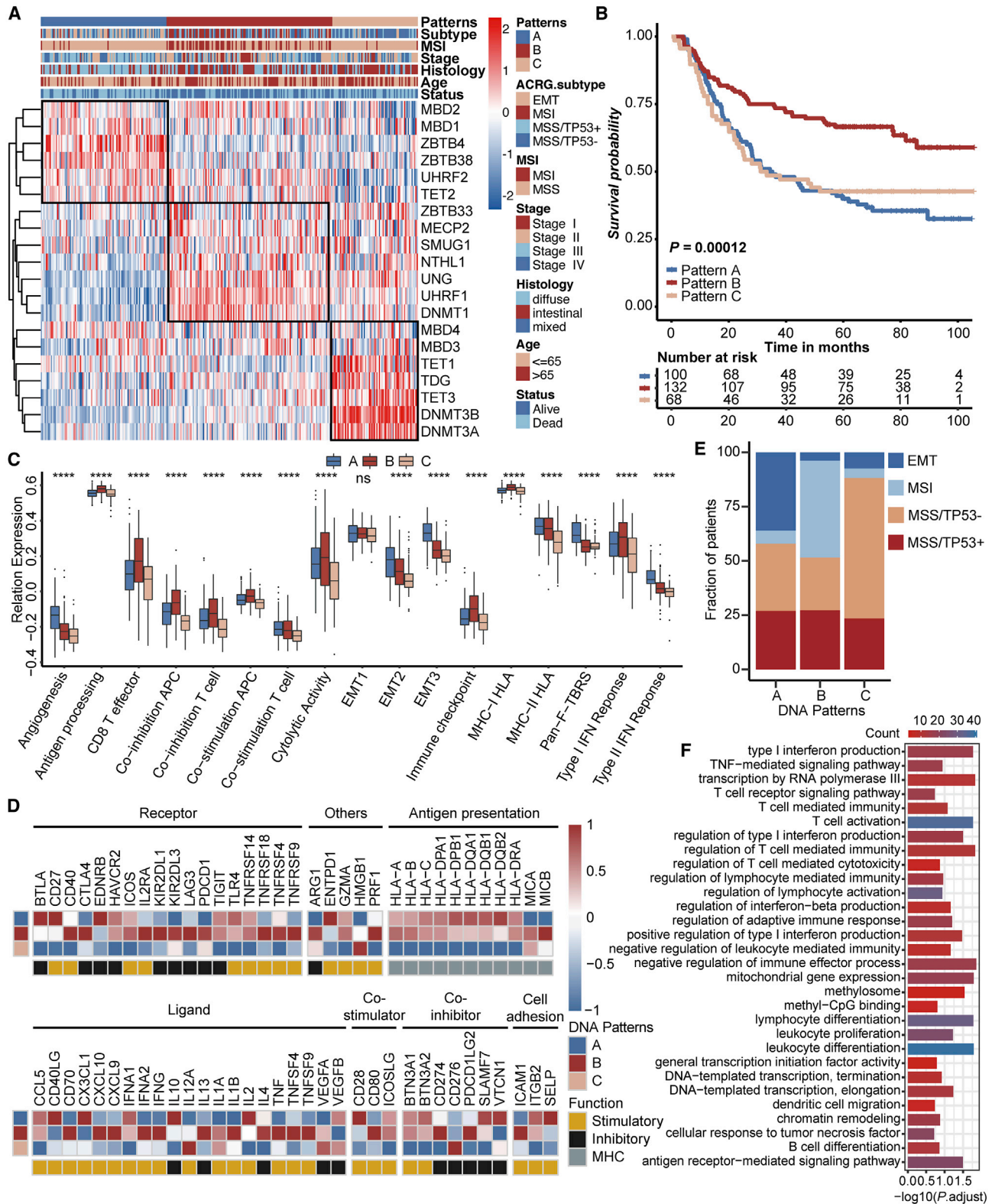
The above results revealed that GC patients could be classified into three immune phenotype groups based on the expression of 20 DNA methylation modifiers. In the three groups, pattern B represented an immune-inflamed phenotype characterized by a relatively hot immune microenvironment and a high proportion of immune cell infiltration. Pattern A represented an immune-excluded phenotype characterized by stroma activation and immune cells surrounding the tumor. Pattern C represented an immune-desert phenotype characterized by little immune cell infiltration and immune repression status.

#### The clinical and transcriptomic characteristics of DNA methylation-related gene clusters and the construction of DMS

To further explore the heterogeneity of different DNA methylation regulator patterns, we recognized the differentially expressed genes (DEGs) among groups. A total of 859 DNA methylation regulator pattern-related genes were identified (Figure S4I). Gene Ontology (GO) analysis showed that the pathways were enriched in immune and DNA methylation-related events (Figure 4F), indicating that the different clinical and transcriptomic characteristics among DNA methylation regulator patterns might result from these differential DNA methylation signature genes. Subsequently, a univariate Cox regression analysis certified that 265 genes had prognostic value (Table S6). Unsupervised clustering analysis based on the expression of these 265 genes also divided GC patients into three clusters, which

#### Figure 3. DNA methylation modification patterns in the gathered GC cohort

(A) The table shows DNA methylation regulators enriched in different DNA methylation regulator patterns. (B) Three-dimensional principal component analysis (3D-PCA) for the expression of 20 DNA methylation regulators to distinguish three DNA methylation regulator patterns in 1,619 patients. (C) Survival analysis of three DNA methylation regulator patterns in 1,619 patients from eight cohorts, including 510 cases of DNA methylation regulator pattern A, 749 cases of DNA methylation regulator pattern B, and 360 cases of DNA methylation regulator pattern C. Log-rank test,  $p < 0.0001$ . (D) Boxplot of relative immune cell abundance for three DNA methylation modification patterns in 1,619 patients. \*\* $p < 0.01$ ; \*\*\*\* $p < 0.0001$ . (E) GSVA analysis of relatively activated hallmark gene sets among three DNA methylation modification patterns. Red represents activated pathways, and blue represents inhibited pathways. The GC cohorts and DNA methylation regulator patterns were used as sample annotations.



(legend on next page)

we called DNA methylation gene clusters (Figures 5A and S5A–S5E). The clinical analysis showed that patients in gene cluster A tended to have an MSI status, earlier staging, and a better histology subtype (Figure 5A). Additionally, survival analysis indicated that gene cluster A had a better prognosis (Figure 5B). In line with the clinical characteristics, patients in gene cluster A presented higher CD8 T effector, co-stimulation of APC, and type I IFN response signatures (Figure S5F) as well as a relatively hot immune microenvironment (Figure 5C). Patients of gene cluster C had higher scores of angiogenesis, pan-F-TBRS, and EMT1-3 signatures (Figure S5F). The result indicated that gene cluster C presented an immune-excluded phenotype as DNA methylation pattern A. Above all, these results reinforced the proposal that there were indeed three different immune phenotype groups in GC, which represented different clinical and immune characteristics.

To evaluate DNA methylation status individually, we further constructed a risk score system based on 265 DNA methylation-related signature genes, that is, the DMS. From this perspective, DNA methylation regulator pattern B showed the highest median DMS, while DNA methylation regulator pattern A showed the lowest median DMS (Figure 5D). For DNA methylation gene clusters, cluster A showed the highest median DMS, while cluster C showed the lowest median DMS (Figure 5E). Among the four ACRG subtypes, the MSI subtype tended to have the highest DMS, while the EMT subtype tended to have the lowest DMS (Figure 5F). With a median cutoff value of 0.0429, we divided the patients into DMS-high and DMS-low groups. The relationship of the DNA methylation regulator pattern, ACRG molecular subtype, gene cluster, and DMS group is summarized in a Sankey diagram (Figure 5G; Table S7).

#### Prognostic value of DMS and validation of GC subtypes in TCGA cohort

Next, we explored the prognostic impact of DMS in GC patients. Survival analysis indicated that the DMS-high group had prolonged survival time in the ACRG cohort (Figure 6A,  $p < 0.0001$ ), which was further validated in TCGA STAD cohort (Figure 6B,  $p = 0.00039$ ). The multivariate Cox regression model confirmed that DMS was an independent prognostic biomarker for evaluating patient survival in both the ACRG and TCGA cohorts (Figures S6A and S6B).

Additionally, we also conducted multi-cohort validation of the prognostic value of DMS. In accord with the results in the ACRG and

TCGA STAD cohorts, the DMS-high group had prolonged overall survival (OS) in the GEO: GSE15459 ( $p = 0.023$ ), GSE26899 ( $p = 0.037$ ), GSE26901 ( $p = 0.0032$ ), and GSE84437 ( $p = 0.014$ ) cohorts, as well as the gathered eight GEO GC cohorts ( $p < 0.0001$ ) (Figures S6C–S6G). Additionally, DMS was also correlated with disease-free survival (DFS), with DMS-high group patients having prolonged DFS ( $p < 0.0001$ ) (Figure S6H). In the three cohorts with recurrence information, DMS was also correlated with recurrence-free survival (RFS) in the GEO: GSE26253 ( $p = 0.0019$ ), GSE26899 ( $p = 0.04$ ), and GSE26901 ( $p = 0.005$ ) cohorts (Figures S6I–S6K).

In addition, DMS could also contribute to evaluating some clinical characteristics. The DMS-high group tended to have more MSI status, earlier staging, and better histology subtypes in the ACRG cohort (Figure 6C). It has been reported that MSI status and EBV-positive phenotype might be related to better immunotherapy efficacy.<sup>25</sup> Of the four TCGA STAD molecular subtypes, the MSI and EBV-positive groups showed higher DMS scores (Figures 6D and S7A). The results of the Seung GC cohort were also in accord with the results of TCGA cohort (Figure S7B).

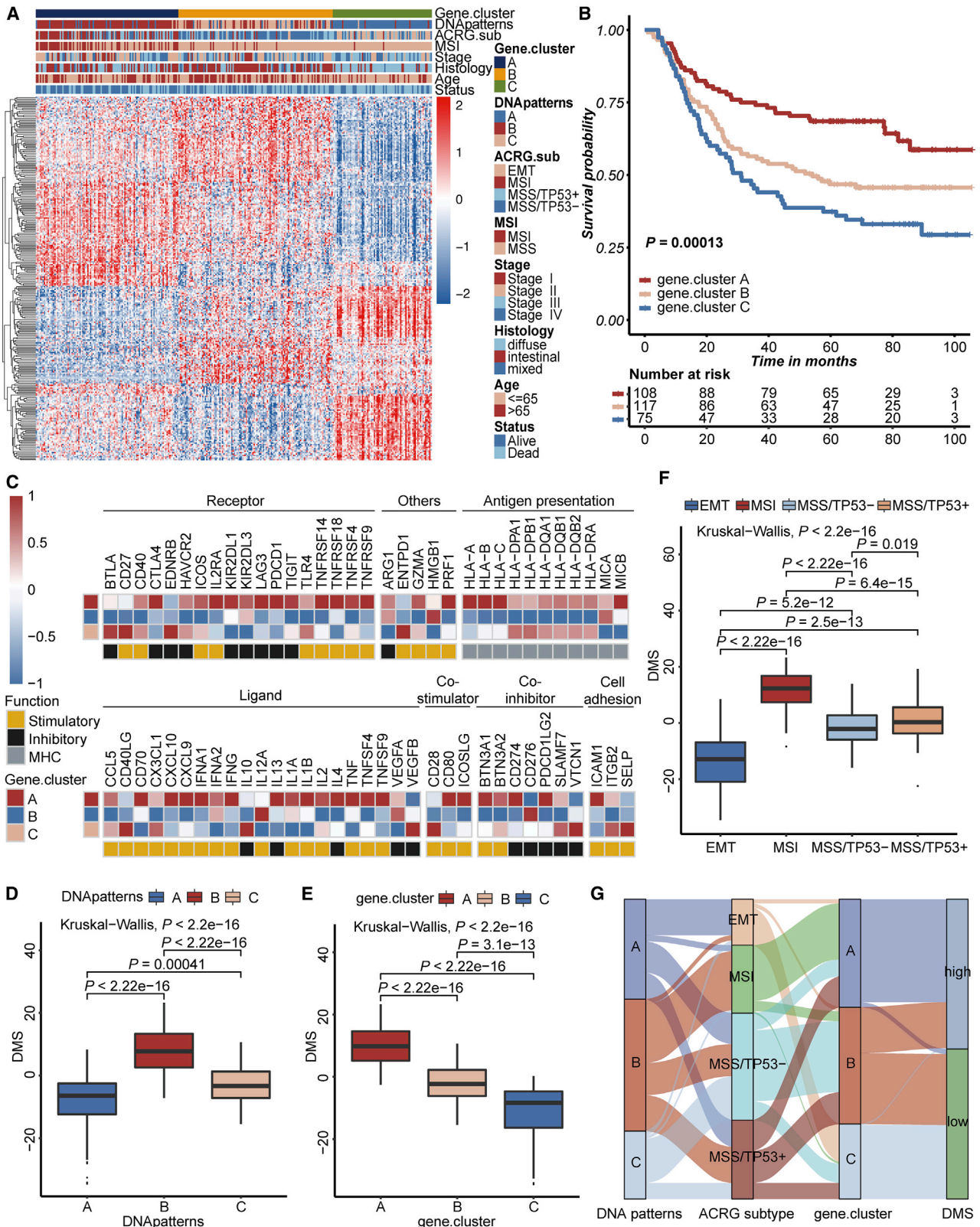
The above results revealed that DMS was a significant prognostic biomarker that could effectively predict OS, DFS, RFS, and some clinical characteristics of GC patients and offer potential clinical application value.

To further investigate the relationship between DNA methylation regulator patterns, DMS, and the methylation status of GC, we first adopted four CIMP subtypes that were annotated by Liu et al.<sup>27</sup> Results showed that patients with CIMP status tended to have high DMS (Figure 6D). Additionally, we also downloaded TCGA STAD 450K data. To our surprise, unsupervised clustering based on the 2,000 most variable transcription start site (TSS) CpG sites also classified patients into three groups (Figure S7C), which we called MethCluster. Survival analysis showed that MethCluster C2 had the best prognosis, with the highest DMS (Figures 6E and S7D). The proportion of immune cells and immune signature analysis showed that MethCluster C2 had relatively high activated CD8 T cell and CD4 T cell abundance and relatively high CD8 effector T cell, cytolytic activity, and antigen presentation pathway scores (Figures S7E and S7F). In addition, MethCluster C2 showed abundant stimulatory or major histocompatibility complex (MHC) molecule expression (Figure S7G), which represented a relatively hot immune

#### Figure 4. Different clinical and transcriptome characteristics of the three DNA methylation regulator patterns in the ACRG cohort

(A) Unsupervised clustering of 20 DNA methylation regulators in the ACRG cohort. Red represents high expression, and blue represents low expression. The DNA methylation regulator patterns, ACRG subtypes, MSI status, stage, histology subtype, age, and survival status were used as sample annotations. (B) Survival analysis of three DNA methylation regulator patterns in the ACRG cohort, including 100 cases of DNA methylation regulator pattern A, 132 cases of DNA methylation regulator pattern B, and 68 cases of DNA methylation regulator pattern C. Log-rank test,  $p < 0.0001$ . (C) Boxplot of several immune signatures for three DNA methylation regulator patterns in the ACRG cohort. \*\*\*\* $p < 0.0001$ . (D) Stacked bar plot of ACRG molecular subtype for three DNA methylation regulator patterns. MSI subtype, light blue; EMT subtype, blue; MSS/TP53<sup>+</sup> subtype, red; MSS/TP53<sup>-</sup> subtype, orange. (E) The heatmap shows the mean differences of immune-related gene expression in the three DNA methylation regulator patterns. The red square indicates upregulation, while the blue square indicates downregulation. Stimulatory molecular, yellow; inhibitory molecular, dark; MHC molecular, gray. (F) Gene Ontology (GO) analysis depicted the enriched pathways of DNA methylation-related genes. The color of the bar plot represents the number of genes enriched in this pathway.





(legend on next page)

microenvironment and might explain its better prognosis. The relationship of DNA methylation regulator patterns, TCGA subtype, CIMP status, MethCluster, and DMS was visualized in an alluvial diagram (Figure 6F). Above all, the results of the DNA methylome further validated that there were three DNA methylation-related molecular subtypes in GC, which revealed the consistency of clustering between the transcriptome and DNA methylome.

Then, we also analyzed the correlation of intrinsic immune escape mechanisms with DMS in TCGA STAD patients. The results showed that TMB and tumor neoantigen burden (TNB) were relatively higher in the DMS-high group, indicating the relatively high immunogenicity (Figures S8A and S8B). While homologous recombination deficiency (HRD), cancer-testis antigen (CTA), aneuploidy score, intratumor heterogeneity (ITH), and stroma fraction were relatively higher in the DMS-low group (Figures S8C–S8G), indicating a higher degree of malignancy and lower immune cell infiltration.

#### Predictive value of DMS in immunotherapy

Immunotherapy has manifested improved survival in the treatment of multiple tumor types, and it is urgent to identify patients who will benefit most. Thus, we further explored whether DMS could predict the efficacy of immunotherapy using four immune checkpoint blockade treatment cohorts.

In the Seung CC cohort, which was the only public transcriptome dataset in GC immunotherapy cohorts to our knowledge, patients in the response group tended to have higher DMS (Figures 7A, 7B, and S9A). It was reported that patients in MSI-H and EBV-positive groups showed higher response rates.<sup>28</sup> In line with this, these patients also exhibited higher DMS (Figure 7C). In addition, the mesenchymal subtype has been demonstrated to be a negative predictor of response to immunotherapy in GC.<sup>28</sup> The mesenchymal subtype showed relatively low DMS in this cohort (Figure S9B). Moreover, we also found a positive correlation between DMS and the expression of PD-L1 (Figure S9C), whose high expression indicated better efficacy of immunotherapy. To our regret, the survival data of the patients in this cohort were not accessible. Thus, three pan-cancer immunotherapy cohorts were further adopted to evaluate the predictive value of DMS. In the UC\_Atezo cohort, with urothelial cancer patients treated with atezolizumab, the high DMS group had prolonged OS ( $p = 0.038$ ) (Figure 7D). At the same time, the partial response (PR) and complete response (CR) groups had relatively higher

DMS (Kruskal-Wallis test,  $p = 0.0014$ ) (Figures 7E, S9D, and S9E). We also evaluated the prognostic prediction efficiency of the combination of TMB and DMS. The results showed that the DMS-high and TMB-high groups had the best overall survival compared with the other groups (Figure 7F). The immune phenotypes in this cohort have been certified by experiments, and so we further investigated the correlation of DMS with three classic immune phenotypes. As shown in Figure 7G, the patients with an immune-inflamed phenotype had the highest DMS, which further confirmed our analysis above. The same results were also found in the PRJEB23709 cohort and David Liu cohort. The DMS-high group exhibited better prognosis and higher clinical response rates (Figures 7H–7K and S9F–S9H).

Importantly, in order to further evaluate the predictive performance of the DMS in GC, we compared the DMS with 10 previously published gene expression immune-related signatures studied in response to immune checkpoint inhibitors (ICIs).<sup>29–35</sup> The results showed that the DMS was the best signature for predicting response to immunotherapy with an area under the curve (AUC) value of 0.843 (Figures 7L and S9I).

Above all, the results of these four immunotherapy cohorts solidly certified that DMS had the ability to efficiently predict the efficacy of immunotherapy and might achieve better predictive value when combined with TMB.

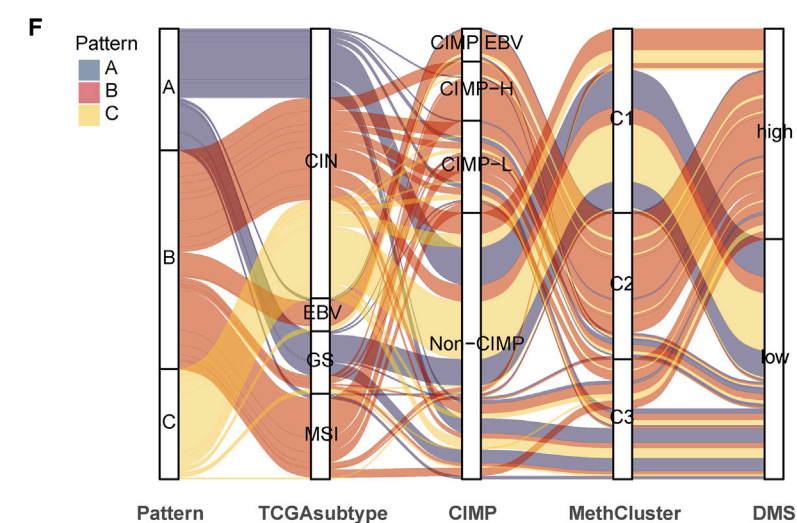
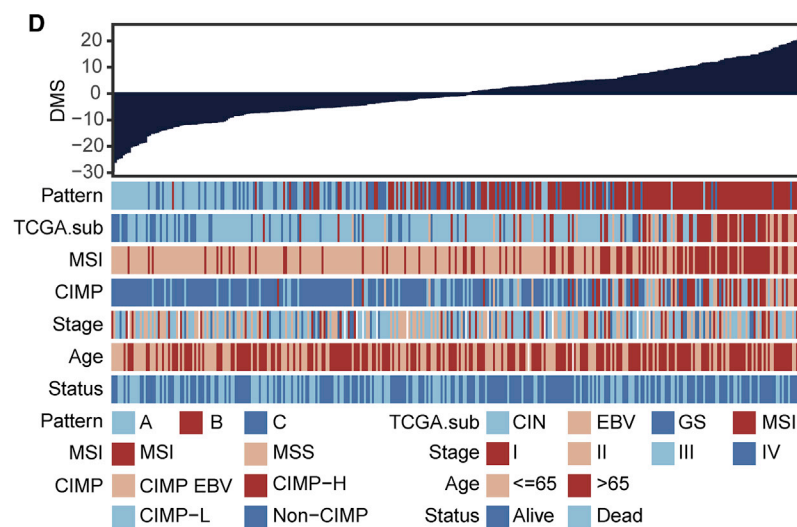
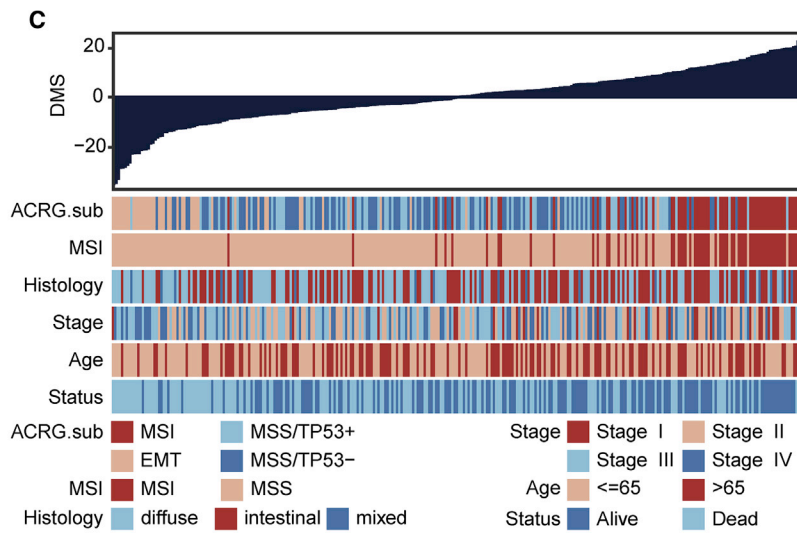
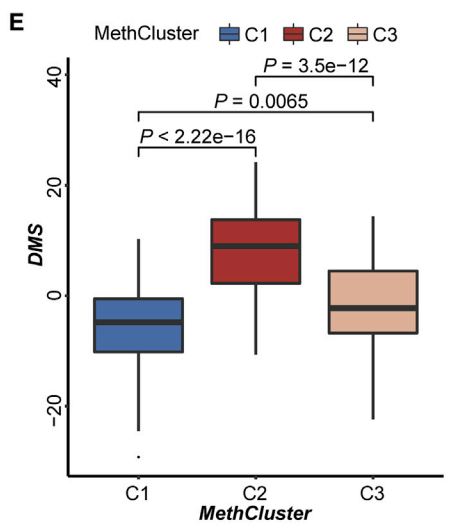
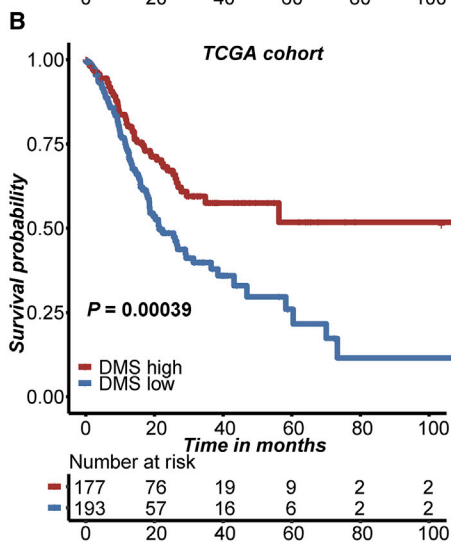
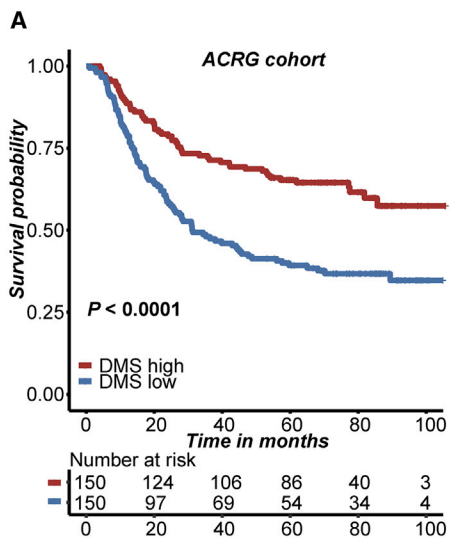
#### DISCUSSION

In recent years, growing evidence has revealed that DNA methylation plays crucial roles in the regulation of antitumor immunity and the response to immunotherapy.<sup>21–23</sup> However, the global profiling of DNA methylation regulator patterns and its impact on the immune microenvironment of GC remains to be clarified. Identifying the relationship between different DNA methylation modification patterns and immune cell infiltration in GC is beneficial to deepen our understanding of the tumor immune microenvironment and to guide more effective immunotherapy strategies.

In this study, we first recognized three DNA methylation regulator patterns that have distinct immune characteristics by unsupervised clustering of the gene expression of DNA methylation regulators. The results were consistent with three classical immune phenotypes: immune-inflamed, immune-excluded, and immune desert.<sup>26</sup> DNA

#### Figure 5. Clinical and transcriptomic characteristics of the DNA methylation gene cluster and the construction of DMS

(A) Unsupervised clustering of 265 DNA methylation-related genes in the ACRG cohort. The top clinical annotation included DNA methylation regulator patterns, ACRG molecular subtypes, MSI status, stage, histology, age, and survival status. Red represents high expression, and blue represents low expression. (B) Survival analysis of three DNA methylation-related gene clusters, including 108 cases in gene cluster A, 117 cases in gene cluster B, and 75 cases in gene cluster C. Log-rank test,  $p = 0.00013$ . (C) Heatmap showing the mean differences of immune-related gene expression in three DNA methylation gene clusters. The red square indicates upregulation, while the blue square indicates downregulation. Stimulatory molecular, yellow; inhibitory molecular, dark; MHC molecular, gray. (D) Boxplot of DMS for three DNA methylation regulator patterns. The upper and lower ends of the boxes represent the interquartile range of values. The lines in the boxes represent the median value, and black dots show outliers. Kruskal-Wallis test,  $p < 0.0001$ . (E) Boxplot of DMS for three DNA methylation gene clusters. Kruskal-Wallis test,  $p < 0.0001$ . (F) Boxplot of DMS for four ACRG molecular subtypes. Kruskal-Wallis test,  $p < 0.0001$ . (G) Sankey diagram depicting the relationship of DNA methylation regulator pattern, ACRG molecular subtype, gene cluster, and DMS group.



(legend on next page)

methylation regulator pattern B was characterized by activation of multiple immune/inflammation-related pathways and a higher proportion of CD8<sup>+</sup> effector cell and APC infiltration. In addition, many stimulatory immunomodulators were generally upregulated, indicating that DNA methylation regulator pattern B had a hot immune microenvironment. In line with this, patients with pattern B had the best prognosis. Contrary to pattern B, DNA methylation regulator pattern C had little immune cell infiltration and extremely low expression of stimulatory immunomodulators or MHC molecules, which revealed a cold microenvironment. Although DNA methylation regulator pattern A also had a high proportion of CD8<sup>+</sup> effector cell and other immune cell infiltration, the activation of the stroma and TGF- $\beta$  pathway hindered the penetration of immune cells into the parenchyma of the tumor, which presented an immune-excluded phenotype. Therefore, it was not surprising that DNA methylation regulator pattern A has poorer prognosis than pattern B.

Furthermore, DEGs among these three DNA methylation regulator patterns were considered DNA methylation-related signature genes and might be directly or indirectly regulated by DNA methylation events. Similar to the results of the DNA methylation regulator patterns, three DNA methylation gene clusters that correlated with immune or stromal activation were recognized based on these DNA methylation signature genes. These results demonstrated that there were indeed three distinct immune subtypes in GC.

Considering the heterogeneity of DNA methylation modification individually, there was a need to quantify the DNA methylation modification profiles of a single tumor. Thus, a DNA methylation-related scoring system called DMS was further constructed and validated in multiple GC datasets. The immune-inflamed subtype has higher DMS, which was further validated in a cohort whose immune phenotype was already determined by experiments.<sup>26</sup> Multivariate analysis also indicated that DMS was an independent prognostic factor in GC. Patients with EBV-positive or MSI status that tended to benefit from immunotherapy<sup>25</sup> had relatively high DMS. In addition, DMS also showed excellent predictive value in multiple immunotherapy cohorts.

We also conducted unsupervised clustering using promoter DNA methylation sites of GC in TCGA. To our surprise, patients were also divided into three clusters. Patients of MethCluster C2 had a high proportion of activated CD4 and CD8 T cell infiltration and a hot immune microenvironment, in line with better prognosis and higher DMS. These results revealed a consistency between the transcriptome and DNA methylome and further validated that there were indeed three distinct immune subtypes in GC.

In view of the clinical significance of our study, we constructed a DMS that can evaluate the DNA methylation profiles individually. The predictive value of DMS for survival was validated in multiple GC cohorts. Additionally, DMS could also be used for assessing the clinicopathological features of patients, such as MSI status, EBV status, histology subtype, molecular subtypes, clinical stages, and TMB, among others. In addition, DMS had the ability to predict the efficacy of PD-1/PD-L1 immune checkpoint blockade therapy, which was validated in a GC immunotherapy cohort and three pan-cancer immunotherapy cohorts. Moreover, when combined with TMB, the widely accepted immunotherapy biomarker DMS revealed better predictive performance. Therefore, DMS might be an excellent biomarker for predicting the efficacy of immune checkpoint therapy and might promote personalized GC immunotherapy in the future.

There were also some limitations to our study. First, the survival data of the GC immunotherapy cohort were not accessible. The predictive performance of DMS for GC needs to be further certified in the future. Second, only the median cutoff of DMS in the ACRG cohort was used to classify the GC, and the optimal cutoff value of the DMS might be needed to better stratify the GC patients.

In conclusion, we identified three distinct immune subtypes in GC from the perspective of DNA methylation and constructed an individual DNA methylation profile scoring system. DMS is a valuable tool for the prediction of survival, clinicopathological characteristics, and the efficacy of immunotherapy and might help to promote personalized GC immunotherapy in the future.

## MATERIALS AND METHODS

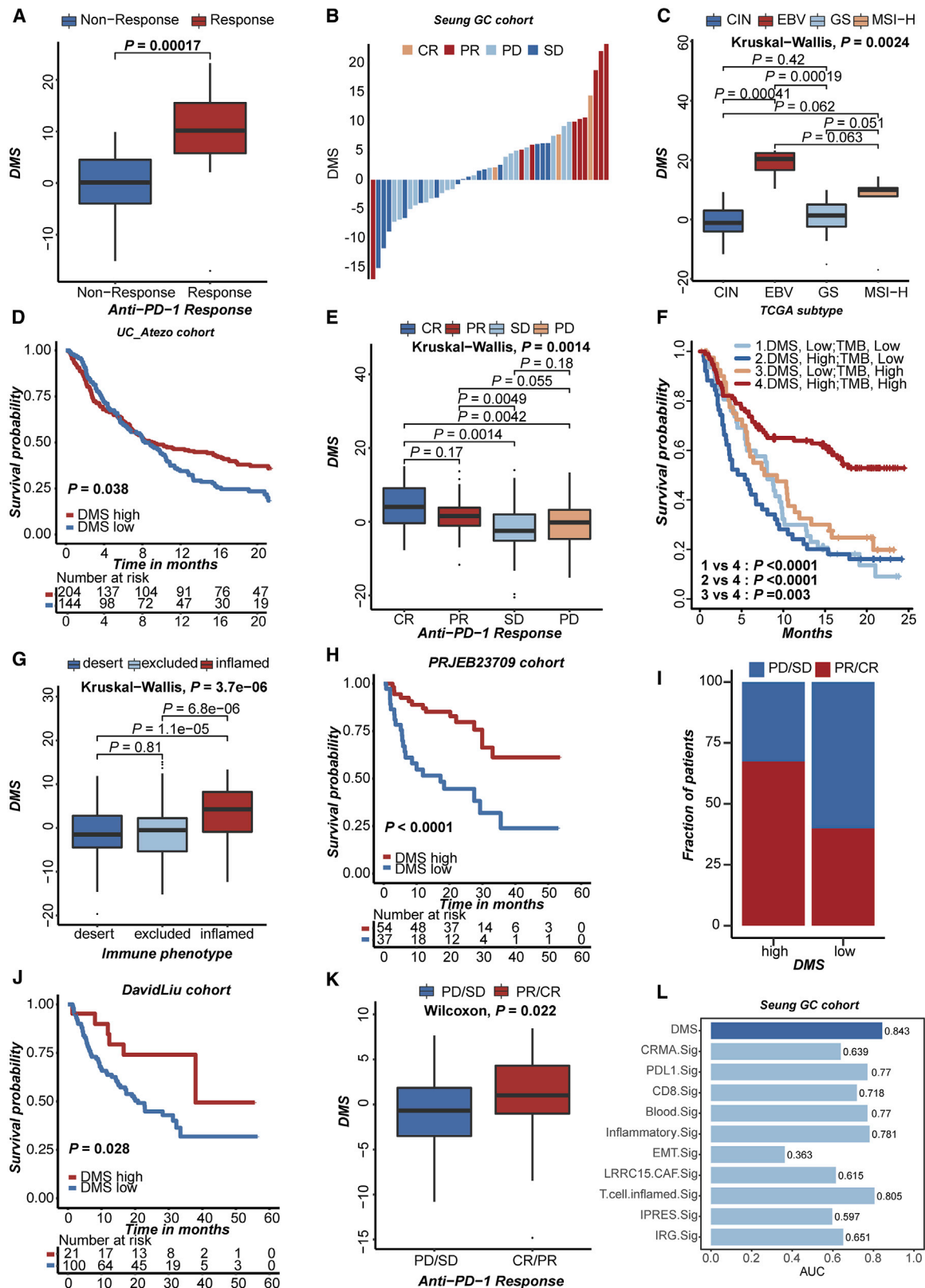
### Collection of GC datasets and preprocessing

The workflow of our work is shown in [Figure S1A](#). Publicly available data from the GEO and TCGA databases were used in this study. Patients without survival information were removed from further evaluation. In total, we gathered eight GC cohorts (ACRG, GEO: GSE15459, GSE34942, GSE57303, GSE84437, GSE26899, and GSE26901, and TCGA) including 1,619 patients for further analysis.

For TCGA STAD cohort, RNA sequencing data (fragments per kilobase of transcript per million mapped reads [FPKM] values) were downloaded via the R package TCGAbiolinks.<sup>36</sup> Then, FPKM values were transformed into transcripts per kilobase million (TPM) values that were more similar to those resulting from microarrays. Somatic mutation (SNPs and small INDELS) and methylation 450K data were downloaded from the University of California Santa Cruz (UCSC) Xena browser (<https://xenabrowser.net>). Clinical data were collected

### Figure 6. Prognostic value of DMS and validation of GC subtypes in TCGA cohort

(A) Survival analysis of the high (n = 150) and low (n = 150) DMS groups in the ACRG cohort based on median value. Log-rank test,  $p < 0.0001$ . (B) Survival analysis of the high (n = 177) and low (n = 193) DMS groups in TCGA STAD cohort. Log-rank test,  $p = 0.00039$ . (C) Bar chart depicting the relationship of DMS and various clinical characteristics in the ACRG cohort. The ACRG subtypes, MSI status, stage, histology subtype, age, and survival status were used as sample annotations. (D) Bar chart depicting the relationship of DMS and various clinical characteristics in TCGA cohort. TCGA subtypes, MSI status, CIMP status, stage, histology subtype, age, and survival status were used as sample annotations. (E) Boxplot of DMS for three MethClusters in TCGA STAD cohort. Kruskal-Wallis test,  $p < 0.0001$ . (F) Alluvial diagram depicting the relationship of DNA methylation regulator pattern, TCGA molecular subtype, CIMP status, MethCluster, and DMS group.



(legend on next page)

from (1) the corresponding GEO dataset metadata, and (2) the supplemental files of relevant articles.<sup>27,37–39</sup> Batch effects resulting from non-biological technical biases were corrected using the ComBat algorithm of the *sva* package. All baseline information of eligible GC datasets is summarized in [Table S1](#).

#### Collection of immune-related data

The immune-related features and genes of TCGA GC patients are available at <https://gdc.cancer.gov/about-data/publications/panimmune>. Four immune checkpoint blockade treatment cohorts with available expression and clinical information were used in our study: (1) Seung GC cohort, metastatic GC with pembrolizumab treatment; (2) David Liu cohort, metastatic melanoma with nivolumab or pembrolizumab treatment; (3) UC\_Atezo cohort, urothelial cancer with atezolizumab treatment; and (4) PRJEB23709 cohort, melanoma with ipilimumab + nivolumab/pembrolizumab or nivolumab/pembrolizumab treatment.

Ten previously published immune related signatures studied in response to ICI were collected to compare with our established signature DMS ([Table S8](#)).

#### Crosstalk among DNA methylation regulators

The protein-protein interactions among DNA regulators were identified based on the STRING<sup>40</sup> interaction database and were further visualized by Cytoscape.<sup>41</sup> The size of a node indicates the modifier numbers interacting with it.

#### Unsupervised clustering for DNA methylation genes

Unsupervised clustering methods were used to identify different DNA methylation modification patterns and classify patients for further analysis. A total of 20 regulators that were collected from published articles were extracted from eight integrated GEO big datasets or the ACRG cohort to identify different DNA modification patterns mediated by DNA methylation modifiers. A consensus clustering algorithm was performed using the R package ConsensusClusterPlus<sup>42</sup> and was repeated 1,000 times in order to ensure the stability of clustering.

#### Gene set variation analysis (GSVA) and single-sample GSEA (ssGSEA)

The R package GSVA<sup>43</sup> was used to quantify the activity of biological pathways. Immune gene signatures were collected from previously

published works.<sup>26,38,44</sup> All hallmark gene sets were downloaded from the Molecular Signature Database (MSigDB) to compare differences between DNA modification patterns. The 10 most common oncogenic hallmarks were obtained from the supplementary table of Sanchez-Vega et al.'s<sup>45</sup> work. The ssGSEA algorithm in the R package GSVA was used to estimate the relative abundance of each immune cell in GC. The gene sets defining each immune cell type were downloaded from the study of Charoentong<sup>46</sup> ([Table S9](#)).

#### DEGs among DNA patterns

DEGs among different DNA modification patterns were determined using the R package limma.<sup>47</sup> The significance criterion for DEGs was set as an adjusted *p* value of <0.01.

#### Functional and pathway enrichment analysis

GO analysis was performed to identify enriched GO terms using the R package clusterProfiler<sup>48</sup> with a cutoff of *p* value of <0.05 and an adjusted *p* value of <0.2. To identify the most related pathways of DNA modifiers, the gseKEGG function of the R package clusterProfiler was used. The DEGs list was estimated between groups with high and low expression of this gene and ordered according to the fold change.

#### Generation of the DMS

First, the prognostic analysis was performed for each gene in the 859 DEGs using a univariate Cox regression model. A total of 265 genes with significant prognosis were extracted for further analysis. Then, the expression of these genes was transformed into a *Z* score. PCA was conducted to construct a DNA methylation relevant score, which we called DMS. Both PC1 and PC2 were selected to serve as signature scores. This method offered the advantage of focusing the score on the set with the largest block of well-correlated (or anticorrelated) genes in the set, while downweighting contributions from genes that do not track with other set members:<sup>38,49</sup>

$$DMS = \sum(PC1_i + PC2_i),$$

where *i* is the expression of DNA methylation regulator pattern-related signature genes.

#### Statistical analysis

The normality of the variables was tested using the Shapiro-Wilk normality test.<sup>50</sup> For comparisons of two normally distributed groups,

#### Figure 7. The role of DMS in four immune checkpoint treatment cohorts

(A) Boxplot of DMS for distinct clinical response groups in the Seung GC immunotherapy cohort. No response, blue; response, red. Wilcoxon test, *p* = 0.00017. (B) Waterfall plot of DMS for distinct clinical response groups in the Seung GC immunotherapy cohort. (C) Boxplot of DMS for different TCGA subtypes in the Seung GC immunotherapy cohort. The MSI-H and EBV groups showed higher DMS. Kruskal-Wallis test, *p* = 0.0024. (D) Survival analysis of the high (*n* = 204) and low (*n* = 144) DMS groups in the UC\_Atezo immunotherapy cohort. Log-rank test, *p* = 0.038. (E) Boxplot of DMS for distinct clinical response groups. The PR and CR groups had relatively higher DMS. Kruskal-Wallis test, *p* = 0.0014. (F) Survival analysis of distinct groups stratified by both TMB and DMS. (G) Boxplot of DMS for three established immune phenotypes in the UC\_Atezo immunotherapy cohort. Kruskal-Wallis test, *p* < 0.001. (H) Survival analysis of the high (*n* = 54) and low (*n* = 37) DMS groups in the PRJEB23709 immunotherapy cohort. Log-rank test, *p* < 0.0001. (I) Stacked bar plot depicting different fractions of clinical response patients in the high and low DMS groups in the PRJEB23709 immunotherapy cohort. PR/CR, red; PD/SD, blue. (J) Survival analysis of the high (*n* = 21) and low (*n* = 100) DMS groups in the David Liu immunotherapy cohort. Log-rank test, *p* = 0.028. (K) Boxplot of DMS for distinct clinical response groups in the David Liu immunotherapy cohort. PD/SD, blue; CR/PR, red. Wilcoxon test, *p* = 0.022. (L) The multiple bar plots for the AUC values of the 11 ICT response signatures.

statistical analysis was performed by unpaired t tests, and for nonnormally distributed variables, statistical analysis was analyzed by a Wilcoxon rank-sum test. For comparisons of three groups, Kruskal-Wallis tests or one-way ANOVA were used as nonparametric or parametric methods, respectively. Correlation coefficients were computed by Spearman and distance correlation analyses. The best cutoff values of each cohort were evaluated using the surv-cutoff function in the survminer package. The survival curves for the prognostic analysis were conducted via the Kaplan-Meier method, and log-rank tests were utilized to judge differences between groups. The univariate Cox regression model was utilized to calculate the hazard ratios (HRs) for DNA regulators and DNA methylation regulator pattern-related genes. All statistical p values were two-sided, with  $p < 0.05$  considered as statistically significant. All statistical analyses were conducted using R 3.6.1 (<https://www.r-project.org/>).

## SUPPLEMENTAL INFORMATION

Supplemental information can be found online at <https://doi.org/10.1016/j.omtn.2021.03.023>.

## ACKNOWLEDGMENTS

This research was supported by the National Key R&D Program of China (2018YFC1313300 and 2018YFC1313304); the National Natural Science Foundation of China (grant nos. 82073377 and 81772587); the Science and Technology Program of Guangdong (2019B020227002); the Natural Science Foundation of Guangdong Province (2018B030306049); the CAMS Innovation Fund for Medical Sciences (CIFMS) (2019-I2M-5-036); the Guangdong Basic and Applied Basic Research Foundation (2020A1515011456); and by the Natural Science Foundation of Guangdong (2021A1515012439). In addition, we would like to thank TCGA Research Network, the UCSC Xena data portal, the biotraine, and all of the authors for making their valuable research data public.

## AUTHOR CONTRIBUTIONS

Q.M., Y.-X.L., D.-Y.R., H.-Q.J., and M.-Z.Q. designed this work. Q.M., Y.-X.C., Y.-X.L., and M.X. analyzed and interpreted the data. Q.M., Y.-X.L., D.-Y.R., and M.X. wrote this manuscript. Y.-X.L., K.Y., Y.W., Z.-X.L., and R.-H.X. edited and revised this manuscript.

## DECLARATION OF INTERESTS

The authors declare no competing interests.

## REFERENCES

- Schübeler, D. (2015). Function and information content of DNA methylation. *Nature* 517, 321–326.
- Li, E., and Zhang, Y. (2014). DNA methylation in mammals. *Cold Spring Harb. Perspect. Biol.* 6, a019133.
- Smith, Z.D., and Meissner, A. (2013). DNA methylation: Roles in mammalian development. *Nat. Rev. Genet.* 14, 204–220.
- Van Cutsem, E., Sagaert, X., Topal, B., Haustermans, K., and Prenen, H. (2016). Gastric cancer. *Lancet* 388, 2654–2664.
- Wang, Y., Lu, J.H., Wang, F., Wang, Y.N., He, M.M., Wu, Q.N., Lu, Y.X., Yu, H.E., Chen, Z.H., Zhao, Q., et al. (2020). Inhibition of fatty acid catabolism augments the efficacy of oxaliplatin-based chemotherapy in gastrointestinal cancers. *Cancer Lett.* 473, 74–89.
- Li, S., Zhuang, Z., Wu, T., Lin, J.C., Liu, Z.X., Zhou, L.F., Dai, T., Lu, L., and Ju, H.Q. (2018). Nicotinamide nucleotide transhydrogenase-mediated redox homeostasis promotes tumor growth and metastasis in gastric cancer. *Redox Biol.* 18, 246–255.
- Higashimori, A., Dong, Y., Zhang, Y., Kang, W., Nakatsu, G., Ng, S.S.M., Arakawa, T., Sung, J.J.Y., Chan, F.K.L., and Yu, J. (2018). Forkhead box F2 suppresses gastric cancer through a novel FOXF2-IRF2BPL- $\beta$ -catenin signaling axis. *Cancer Res.* 78, 1643–1656.
- Murphy, G., Pfeiffer, R., Camargo, M.C., and Rabkin, C.S. (2009). Meta-analysis shows that prevalence of Epstein-Barr virus-positive gastric cancer differs based on sex and anatomic location. *Gastroenterology* 137, 824–833.
- Fattahi, S., Kosari-Monfared, M., Ghadami, E., Golpour, M., Khodadadi, P., Ghasemian, M., and Akhavan-Niaki, H. (2018). Infection-associated epigenetic alterations in gastric cancer: New insight in cancer therapy. *J. Cell. Physiol.* 233, 9261–9270.
- Hugo, W., Zaretsky, J.M., Sun, L., Song, C., Moreno, B.H., Hu-Lieskovan, S., Berent-Maoz, B., Pang, J., Chmielowski, B., Cherry, G., et al. (2017). Genomic and transcriptomic features of response to anti-PD-1 therapy in metastatic melanoma. *Cell* 168, 542.
- Ferris, R.L., Blumenschein, G., Jr., Fayette, J., Guigay, J., Colevas, A.D., Licitra, L., Harrington, K., Kasper, S., Vokes, E.E., Even, C., et al. (2016). Nivolumab for recurrent squamous-cell carcinoma of the head and neck. *n. engl. j. med.* 375, 1856–1867.
- rizvi, n.a., hellmann, m.d., Snyder, A., Kvistborg, P., Makarov, V., Havel, J.J., Lee, W., Yuan, J., Wong, P., Ho, T.S., et al. (2015). Mutational landscape determines sensitivity to PD-1 blockade in non-small cell lung cancer. *Science* 348, 124–128.
- Brahmer, J., Reckamp, K.L., Baas, P., Crinò, L., Eberhardt, W.E., Poddubskaia, E., Antonia, S., Pluzanski, A., Vokes, E.E., Holgado, E., et al. (2015). Nivolumab versus docetaxel in advanced squamous-cell non-small-cell lung cancer. *N. Engl. J. Med.* 373, 123–135.
- Shitara, K., Özgüroğlu, M., Bang, Y.J., Di Bartolomeo, M., Mandalà, M., Ryu, M.H., Fornaro, L., Olesiński, T., Caglevic, C., Chung, H.C., et al.; KEYNOTE-061 investigators (2018). Pembrolizumab versus paclitaxel for previously treated, advanced gastric or gastro-oesophageal junction cancer (KEYNOTE-061): A randomised, open-label, controlled, phase 3 trial. *Lancet* 392, 123–133.
- Fuchs, C.S., Doi, T., Jang, R.W., Muro, K., Satoh, T., Machado, M., Sun, W., Jalal, S.I., Shah, M.A., Metges, J.P., et al. (2018). Safety and efficacy of pembrolizumab monotherapy in patients with previously treated advanced gastric and gastroesophageal junction cancer: Phase 2 clinical KEYNOTE-059 trial. *JAMA Oncol.* 4, e180013.
- Kang, Y.K., Boku, N., Satoh, T., Ryu, M.H., Chao, Y., Kato, K., Chung, H.C., Chen, J.S., Muro, K., Kang, W.K., et al. (2017). Nivolumab in patients with advanced gastric or gastro-oesophageal junction cancer refractory to, or intolerant of, at least two previous chemotherapy regimens (ONO-4538-12, ATTRACTION-2): A randomised, double-blind, placebo-controlled, phase 3 trial. *Lancet* 390, 2461–2471.
- Muro, K., Chung, H.C., Shankaran, V., Geva, R., Catenacci, D., Gupta, S., Eder, J.P., Golan, T., Le, D.T., Burtness, B., et al. (2016). Pembrolizumab for patients with PD-L1-positive advanced gastric cancer (KEYNOTE-012): A multicentre, open-label, phase 1b trial. *Lancet Oncol.* 17, 717–726.
- Wang, F., Wei, X.L., Wang, F.H., Xu, N., Shen, L., Dai, G.H., Yuan, X.L., Chen, Y., Yang, S.J., Shi, J.H., et al. (2019). Safety, efficacy and tumor mutational burden as a biomarker of overall survival benefit in chemo-refractory gastric cancer treated with toripalimab, a PD-1 antibody in phase Ib/II clinical trial NCT02915432. *Ann. Oncol.* 30, 1479–1486.
- Jones, P.A., Ohtani, H., Chakravarthy, A., and De Carvalho, D.D. (2019). Epigenetic therapy in immune-oncology. *Nat. Rev. Cancer* 19, 151–161.
- Dunn, J., and Rao, S. (2017). Epigenetics and immunotherapy: The current state of play. *Mol. Immunol.* 87, 227–239.
- Chiappinelli, K.B., Zahnow, C.A., Ahuja, N., and Baylin, S.B. (2016). Combining epigenetic and immunotherapy to combat cancer. *Cancer Res.* 76, 1683–1689.
- Wu, H.X., Chen, Y.X., Wang, Z.X., Zhao, Q., He, M.M., Wang, Y.N., Wang, F., and Xu, R.H. (2019). Alteration in TET1 as potential biomarker for immune checkpoint blockade in multiple cancers. *J. Immunother. Cancer* 7, 264.

23. Xu, Y.P., Lv, L., Liu, Y., Smith, M.D., Li, W.C., Tan, X.M., Cheng, M., Li, Z., Bovino, M., Aubé, J., and Xiong, Y. (2019). Tumor suppressor TET2 promotes cancer immunity and immunotherapy efficacy. *J. Clin. Invest.* *129*, 4316–4331.
24. Kastan, M.B., and Bartek, J. (2004). Cell-cycle checkpoints and cancer. *Nature* *432*, 316–323.
25. Panda, A., Mehnert, J.M., Hirshfield, K.M., Riedlinger, G., Damare, S., Saunders, T., Kane, M., Sokol, L., Stein, M.N., Poplin, E., et al. (2018). Immune activation and benefit from avelumab in EBV-positive gastric cancer. *J. Natl. Cancer Inst.* *110*, 316–320.
26. Mariathasan, S., Turley, S.J., Nickles, D., Castiglioni, A., Yuen, K., Wang, Y., Kadel, E.E., III, Koeppen, H., Astarita, J.L., Cubas, R., et al. (2018). TGF $\beta$  attenuates tumour response to PD-L1 blockade by contributing to exclusion of T cells. *Nature* *554*, 544–548.
27. Liu, Y., Sethi, N.S., Hinoue, T., Schneider, B.G., Cherniack, A.D., Sanchez-Vega, F., Seoane, J.A., Farshidfar, F., Bowlby, R., Islam, M., et al.; Cancer Genome Atlas Research Network (2018). Comparative molecular analysis of gastrointestinal adenocarcinomas. *Cancer Cell* *33*, 721–735.e8.
28. Kim, S.T., Cristescu, R., Bass, A.J., Kim, K.M., Odegaard, J.I., Kim, K., Liu, X.Q., Sher, X., Jung, H., Lee, M., et al. (2018). Comprehensive molecular characterization of clinical responses to PD-1 inhibition in metastatic gastric cancer. *Nat. Med.* *24*, 1449–1458.
29. Jiang, P., Gu, S., Pan, D., Fu, J., Sahu, A., Hu, X., Li, Z., Traugh, N., Bu, X., Li, B., et al. (2018). Signatures of T cell dysfunction and exclusion predict cancer immunotherapy response. *Nat. Med.* *24*, 1550–1558.
30. Shukla, S.A., Bachireddy, P., Schilling, B., Galonska, C., Zhan, Q., Bango, C., Langer, R., Lee, P.C., Gusenleitner, D., Keskin, D.B., et al. (2018). Cancer-germline antigen expression discriminates clinical outcome to CTLA-4 blockade. *Cell* *173*, 624–633.e8.
31. Yang, S., Wu, Y., Deng, Y., Zhou, L., Yang, P., Zheng, Y., Zhang, D., Zhai, Z., Li, N., Hao, Q., et al. (2019). Identification of a prognostic immune signature for cervical cancer to predict survival and response to immune checkpoint inhibitors. *OncoImmunology* *8*, e1659094.
32. Dominguez, C.X., Müller, S., Keerthivasan, S., Koeppen, H., Hung, J., Gierke, S., Breart, B., Foreman, O., Bainbridge, T.W., Castiglioni, A., et al. (2020). Single-cell RNA sequencing reveals stromal evolution into LRRC15<sup>+</sup> myofibroblasts as a determinant of patient response to cancer immunotherapy. *Cancer Discov.* *10*, 232–253.
33. Huang, A.C., Orłowski, R.J., Xu, X., Mick, R., George, S.M., Yan, P.K., Manne, S., Kraya, A.A., Wubbenhorst, B., Dorfman, L., et al. (2019). A single dose of neoadjuvant PD-1 blockade predicts clinical outcomes in resectable melanoma. *Nat. Med.* *25*, 454–461.
34. Thompson, J.C., Hwang, W.T., Davis, C., Deshpande, C., Jeffries, S., Rajpurohit, Y., Krishna, V., Smirnov, D., Verona, R., Lorenzi, M.V., et al. (2020). Gene signatures of tumor inflammation and epithelial-to-mesenchymal transition (EMT) predict responses to immune checkpoint blockade in lung cancer with high accuracy. *Lung Cancer* *139*, 1–8.
35. Friedlander, P., Wassmann, K., Christenfeld, A.M., Fisher, D., Kyi, C., Kirkwood, J.M., Bhardwaj, N., and Oh, W.K. (2017). Whole-blood RNA transcript-based models can predict clinical response in two large independent clinical studies of patients with advanced melanoma treated with the checkpoint inhibitor, tremelimumab. *J. Immunother. Cancer* *5*, e7.
36. Colaprico, A., Silva, T.C., Olsen, C., Garofano, L., Cava, C., Garolini, D., Sabedot, T.S., Malta, T.M., Pagnotta, S.M., Castiglioni, I., et al. (2016). TCGAAbilinks: An R/Bioconductor package for integrative analysis of TCGA data. *Nucleic Acids Res.* *44*, e71.
37. Liu, J., Lichtenberg, T., Hoadley, K.A., Poisson, L.M., Lazar, A.J., Cherniack, A.D., Kovatich, A.J., Benz, C.C., Levine, D.A., Lee, A.V., et al.; Cancer Genome Atlas Research Network (2018). An integrated TCGA pan-cancer clinical data resource to drive high-quality survival outcome analytics. *Cell* *173*, 400–416.e11.
38. Zeng, D., Li, M., Zhou, R., Zhang, J., Sun, H., Shi, M., Bin, J., Liao, Y., Rao, J., and Liao, W. (2019). Tumor microenvironment characterization in gastric cancer identifies prognostic and immunotherapeutically relevant gene signatures. *Cancer Immunol. Res.* *7*, 737–750.
39. Oh, S.C., Sohn, B.H., Cheong, J.H., Kim, S.B., Lee, J.E., Park, K.C., Lee, S.H., Park, J.L., Park, Y.Y., Lee, H.S., et al. (2018). Clinical and genomic landscape of gastric cancer with a mesenchymal phenotype. *Nat. Commun.* *9*, 1777.
40. Szklarczyk, D., Gable, A.L., Lyon, D., Junge, A., Wyder, S., Huerta-Cepas, J., Simonovic, M., Doncheva, N.T., Morris, J.H., Bork, P., et al. (2019). STRING v11: Protein-protein association networks with increased coverage, supporting functional discovery in genome-wide experimental datasets. *Nucleic Acids Res.* *47* (D1), D607–D613.
41. Shannon, P., Markiel, A., Ozier, O., Baliga, N.S., Wang, J.T., Ramage, D., Amin, N., Schwikowski, B., and Ideker, T. (2003). Cytoscape: A software environment for integrated models of biomolecular interaction networks. *Genome Res.* *13*, 2498–2504.
42. Wilkerson, M.D., and Hayes, D.N. (2010). ConsensusClusterPlus: A class discovery tool with confidence assessments and item tracking. *Bioinformatics* *26*, 1572–1573.
43. Hänzelmann, S., Castelo, R., and Guinney, J. (2013). GSVA: Gene set variation analysis for microarray and RNA-seq data. *BMC Bioinformatics* *14*, 7.
44. Zhang, B., Wu, Q., Li, B., Wang, D., Wang, L., and Zhou, Y.L. (2020). m<sup>6</sup>A regulator-mediated methylation modification patterns and tumor microenvironment infiltration characterization in gastric cancer. *Mol. Cancer* *19*, 53.
45. Sanchez-Vega, F., Mina, M., Armenia, J., Chatila, W.K., Luna, A., La, K.C., Dimitriadou, S., Liu, D.L., Kantheti, H.S., Saghaforia, S., et al.; Cancer Genome Atlas Research Network (2018). Oncogenic signaling pathways in The Cancer Genome Atlas. *Cell* *173*, 321–337.e10.
46. Charoentong, P., Finotello, F., Angelova, M., Mayer, C., Efremova, M., Rieder, D., et al. (2017). Pan-cancer Immunogenomic Analyses Reveal Genotype-Immunophenotype Relationships and Predictors of Response to Checkpoint Blockade. *Cell Rep.* *18*, 248–262.
47. Ritchie, M.E., Phipson, B., Wu, D., Hu, Y., Law, C.W., Shi, W., and Smyth, G.K. (2015). limma powers differential expression analyses for RNA-sequencing and microarray studies. *Nucleic Acids Res.* *43*, e47.
48. Yu, G., Wang, L.G., Han, Y., and He, Q.Y. (2012). clusterProfiler: An R package for comparing biological themes among gene clusters. *OMICS* *16*, 284–287.
49. Sotiropoulos, C., Wirapati, P., Loi, S., Harris, A., Fox, S., Smeds, J., Nordgren, H., Farmer, P., Praz, V., Haibe-Kains, B., et al. (2006). Gene expression profiling in breast cancer: Understanding the molecular basis of histologic grade to improve prognosis. *J. Natl. Cancer Inst.* *98*, 262–272.
50. Ghasemi, A., and Zahediasl, S. (2012). Normality tests for statistical analysis: a guide for non-statisticians. *Int. J. Endocrinol. Metab.* *10*, 486–489.